



Removal of reactive blue 19 from aqueous solutions using NiO nanoparticles: equilibrium and kinetic studies

Zahra Monsef Khoshhesab*, Monavar Ahmadi

Department of Chemistry, Payame Noor University, Tehran, I.R. of Iran, email: monsef_kh@pnu.ac.ir (Z. Monsef Khoshhesab), ahmadi.ch90@yahoo.com (M. Ahmadi)

Received 14 January 2015; Accepted 24 September 2015

ABSTRACT

Adsorption of reactive blue 19 (RB19) dye onto NiO nanoparticles was investigated at various NiO dosages, dye concentrations, solution pHs, contact times, and temperatures in a batch system. Analysis of the adsorption data indicated that the adsorption process follows the pseudo-second-order kinetics and the adsorption equilibrium data fit to Langmuir–Freundlich (Sips) isotherm better than the Freundlich and Langmuir isotherm models. Evaluation of the thermodynamic parameters (ΔG° , ΔH° , and ΔS°) revealed that the adsorption process is spontaneous, endothermic, and feasible. This study suggested NiO nanoparticles as effective adsorbents for removing RB19 from polluted water.

Keywords: Anthraquinone dye; Nanoparticles; NiO; Reactive blue 19; Removal

1. Introduction

The discharge of dyes into wastewaters from coloring industries (particularly the textile industry) is one of the major environmental problems, because not only does it damage the esthetic nature of the contaminated water, but also causes inhibitory effect on photosynthesis activity in aquatic systems. In addition, some dyes may degrade into the compounds, causing toxic, mutagenic, and carcinogenic effects on living organisms [1,2]. Therefore, from health and environmental viewpoints, it is very important to remove the dyes from industrial effluents, before being released to the environment.

Various physicochemical and biological methods have been developed to treat the dye-containing wastewater, including ion-exchange [3], coagulation/flocculation [4,5], ozonation [6], electrochemical/

chemical oxidation [7,8], photocatalysis [9], membrane filtration [10], adsorption [11,12], and microbial biodegradation [13]. However, most of the dyes used in the textile industry are difficult to be removed by conventional physicochemical and biological treatment methods, since they are stable against the light and oxidizing agents and resist biodegradation [14]. Therefore, the adsorption process becomes one of the efficient methods to remove these dyes from effluent. Several synthetic and natural materials such as clay, activated carbon, polymers, zeolite, and agricultural waste have been developed as adsorbents for water treatment [11,15–18]. Among these materials, although activated carbon is one of the most commonly used adsorbent for water treatment, it suffers from some drawbacks such as high cost of operation, slow adsorption kinetics, and low adsorption capacity of bulky adsorbates which restrict its application to remove dyes [19,20]. Hence, it is very important to

*Corresponding author.

exploit new adsorbents with high adsorption capacity as well as low cost. In recent years, nano-structured materials have attracted extensive attention for adsorption processes because of their high surface area, providing fast kinetics and high adsorption capacity [21–26].

NiO is an important transition metal oxide which has received considerable attention because of its extensive applications in catalysts, supercapacitors, lithium-ion batteries, gas-sensors, electrochromic films, and magnetic materials. Moreover, it is a p-type semiconductor with a wide band gap (3.5 eV) which can be used for photocatalytic processes [27]. Many literatures have reported the synthesis of NiO with different morphologies and evaluated their potential applications in various fields [28]. For example, NiO nanoparticles were reported for the photocatalytic degradation of organic pollutants such as chlorinated phenols and crystal violet [29]. As an adsorbent in water treatment, Chen et al. [30] synthesized porous NiO nanosheets and nanoparticles by a chemical precipitation method that exhibited excellent performance for the removal of congo red. Song, et al. [31] utilized NiO (111) nanosheets for the removal of reactive brilliant red X-3B, congo red, and fuchsin acid which exhibited desirable properties in water treatment. Zhu et al. [32] synthesized hierarchical NiO spheres by a thermal method and demonstrated their high adsorption capacities for removal of organic dyes from wastewater. Zhang et al. [33] have reported the hierarchical NiO hollow microsphere synthesis with high adsorption affinity toward congo red in water. More recently, Ai and Zeng [34] have prepared hierarchical porous NiO architectures via a facile additive-free solvothermal route which were found to be efficient adsorbents for removing dye from aqueous solutions.

Reactive blue 19 is an anthraquinone-based vinyl-sulphone dye, extensively used in dyeing of cellulosic fibers. Anthraquinone-based dyes are very resistant to chemical and biological degradation due to their aromatic anthraquinone structure which is highly stabilized by resonance [35]. Thus, they can persist for a long time in wastewater and pose serious environmental problems. Regarding the chemical stability and low biodegradability of RB19, its removal from dyeing effluents and wastewater by a physical method such as adsorption becomes very important to decrease its impact on the environment.

In this study, attempt has been made to explore the application of NiO nanoparticles for removal of RB19 dye from aqueous solutions. The advantages of the NiO nanoparticles are low-cost and simplicity of preparation. The effects of various experimental parameters, including dye solution pH, initial dye

concentrations, adsorbent dosage, and contact time on the adsorption process were studied and optimized. The adsorption isotherms and kinetic studies were also conducted to clarify the adsorption process.

2. Experimental

2.1. Materials and equipment

Reactive blue 19 (RB19) was purchased from the DyeStar Co. (Germany) and used without further purification. The main properties of RB19 were summarized in Table 1. NiO powder obtained from Loba Chemie Co. (India). All other reagents and chemicals were analytical grade and used as received. Deionized water was used throughout the experiments for all solution preparations. Stock solution of dye ($1,000 \text{ mg L}^{-1}$) was prepared by dissolving an accurately weighed quantity of RB19 in deionized water. All of the working solutions were prepared by step-wise diluting of the stock solution with deionized water. To adjust the pH of the solutions, NaOH or HCl (0.10 mol L^{-1}) solutions were used.

A double beam UV–vis spectrophotometer (Shimadzu, UV-1600, Japan) with a 1 cm cell was used for measuring the absorbance. A Metrohm pH meter (827 model) with a combined glass electrode was used for measuring the solution pHs. The prepared nano-NiO was characterized by X-ray diffractometer (XRD; Philips, PW1800) using Cu-K α radiation ($\lambda = 0.15418 \text{ nm}$, 40 kV, 30 mA), transmission electron microscope (TEM, Philips EM208S model), and scanning electron microscope (SEM) using a Philips XLS30 model. Specific surface area and porosity analysis for the prepared NiO nanoparticles were performed through measuring Brunauer–Emmett–Teller (BET) nitrogen adsorption–desorption isotherms at 77 K with a Belsorp mini II (Japan) apparatus. A magnetic stirrer (Heidolph model MR 3001 K) was used for mixing the adsorbent and the dye solutions.

2.2. Preparation of NiO nanoparticles

Nickel oxide nanoparticles were prepared using the procedure as described previously [36]. Briefly, 2.1 g of commercial NiO powder (surface area $7 \text{ m}^2 \text{ g}^{-1}$, particle size $12 \mu\text{m}$) was added into 6.0 mL NH_4HCO_3 aqueous solution (40% w/v) under vigorous stirring at 60°C in two steps: (a) 0.7 g of NiO was added to the prepared NH_4HCO_3 solution until dissolution being completed, (b) the rest of NiO (1.4 g) and 0.04 g of $\text{CO}(\text{NH}_2)_2$ was sequentially added into the above solution and the mixture was stirred for another 2 h. Finally, the green-black precipitate was dried at

Table 1
The main properties of RB 19

Commercial name	Remazol Brilliant Blue R
Chemical formula	$C_{22}H_{16}O_{11}N_2S_3Na_2$
Class	Anthraquinone
Chemical index (C.I.) number	61,200
Molecular weight ($g\ mol^{-1}$)	626.5
λ_{max} (nm)	592
Chemical structure	

60°C for 24 h, and calcinated at 400°C for 1 h to prepare the nano-sized NiO. The NiO nanoparticles with average particle size of 20 nm were used as an adsorbent.

2.3. Adsorption experiments

Batch adsorption studies were conducted by adding a known amount of adsorbent into 250 mL Erlenmeyer flasks containing 50 mL of the dye solution. The prepared suspension was immediately placed on a magnetic stirrer (120 rpm) at room temperature for a predefined time. After appropriate time, the adsorbent was removed by filtration and the filtrates were analyzed for the residual concentration of RB19 dye. The concentration of the dye in solution was determined from the calibration curve prepared by measuring different predetermined concentrations of RB19 solutions at a wavelength corresponding to maximum absorbance of the dye ($\lambda_{max} = 592\ nm$) using UV-vis spectrophotometer. The adsorption percent, i.e. the dye removal efficiency (R) was calculated using the following equation (Eq. (1)):

$$R(\%) = \frac{C_0 - C_t}{C_0} \times 100 \quad (1)$$

where C_0 is the initial concentration ($mg\ L^{-1}$) of dye and C_t is the concentration of dye after a certain period of time ($mg\ L^{-1}$). To check the possible adsorption of RB19 by filtration, a control dye solution (in the absence of NiO nanoparticles) was passed through the filter paper in parallel with each experiment under

the same conditions. In general, the percentage of dye adsorption by filtration was lower than <3%.

The adsorption kinetics and adsorption isotherm were performed using a thermostatic bath at constant temperature ($25^\circ C \pm 0.5$) and at natural pH of the dye solution (pH ~ 6.5). To study the adsorption kinetics of RB19 onto NiO nanoparticles, 0.11 g of NiO nanoparticles adsorbent was added into 50 mL of $75\ mg\ L^{-1}$ RB19 solutions and the suspensions were agitated for different times. The suspensions were then filtrated and the dye concentration in each supernatant solution was determined. Adsorption isotherm studies were conducted by mixing 0.11 g of NiO nanoparticles with 50 mL of the dye solutions of different concentrations varying from 25 to $500\ mg\ L^{-1}$ for 60 min of agitation time at 25, 35, and 45°C. After that, the suspensions were filtrated and the dye concentration in each supernatant solution was determined using UV-vis spectrophotometer. The amount of RB19 adsorbed per unit mass of NiO nanoparticles adsorbent at equilibrium was calculated from the following equation:

$$q_e = \frac{(C_0 - C_e) \times V}{m} \quad (2)$$

where q_e is the adsorption capacity ($mg\ g^{-1}$); C_0 and C_e are the initial and equilibrium concentrations of RB19 ($mg\ L^{-1}$); V is the volume of RB19 solution (L), and m is the mass of NiO nanoparticles adsorbent (g). The influence of filtration on the dye adsorption was compensated by a control dye solution used in parallel with each experiment. For this purpose, a dye solution

(in the absence of adsorbent) was passed through the filter paper and its concentration after filtration was used for calculation of q_e (or R %). All experiments were carried out in triplicate and the mean values were presented. The maximum RSD (relative standard deviation) was less than 4%.

3. Results and discussion

3.1. Characterization of NiO nanoparticles

The XRD spectrum, TEM, and SEM images were used to characterize the crystalline phase, size, and morphology of the prepared NiO nanoparticles. As shown in Fig. 1, the diffraction peaks appeared at 2θ of 37.30° , 43.32° , 62.88° , 75.40° , and 79.53° can be indexed as (1 1 1), (2 0 0), (2 2 0), (3 1 1), and (2 2 2) crystal planes of the cubic crystalline structure of NiO (JCPDS Card No. 04-0835). No characteristic peaks of impurities are detected, indicating high purity of the prepared NiO. The crystallite size of the prepared NiO nanoparticles was calculated using the Scherrer formula: $D_c = K\lambda/\beta_{1/2} \cos\theta$ [37]. Where D_c is the crystallite diameter, K is the Scherrer constant (0.89), λ is the X-ray wavelength (0.15418 nm), $\beta_{1/2}$ is the full width at half maximum (FWHM) of the diffraction peak, and θ is the diffraction angle of the peak. The average crystallite size of the prepared NiO, calculated from the diffraction peaks (1 1 1), (2 0 0), and (2 2 0), was found to be about 20 nm. Fig. 2 shows the TEM image of the NiO nanoparticles. The size of the particles is typically in the range of 15–30 nm and most of the nanoparticles have size around 20 nm. These results confirm the preparation of pure crystalline and nano-sized NiO. The SEM image (Fig. 3) shows a quasi spherical morphology of the prepared NiO nanoparticles. The textural properties of the prepared NiO nanoparticles were investigated by N_2

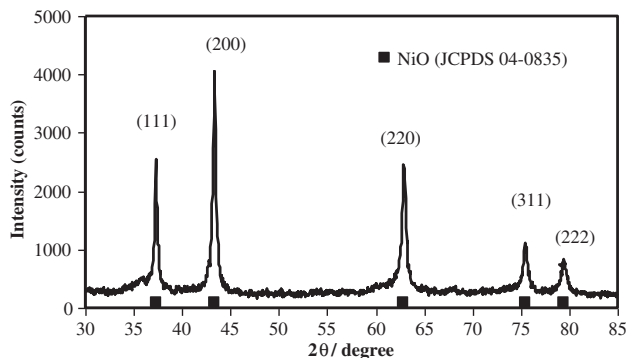


Fig. 1. The XRD pattern of the prepared NiO nanoparticles.

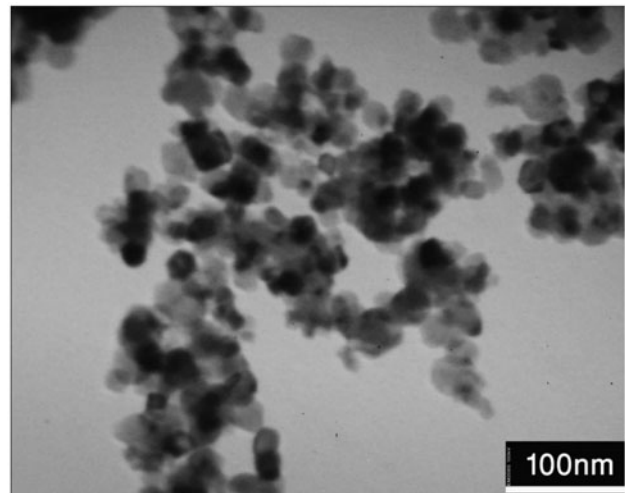


Fig. 2. The TEM image of the prepared NiO nanoparticles.

adsorption/desorption isotherm and corresponding Barrett–Joyner–Halenda (BJH) pore size distribution (inset) obtained from the adsorption branch are shown in Fig. 4. BET surface area and porosity parameters of the NiO nanoparticles are given in Table 2. This isotherm profile can be categorized as type IV hysteresis loop, indicating the presence of a mesoporous structure in the sample [38].

3.2. Adsorption of RB 19 by NiO nanoparticles

To obtain the optimal conditions for the removal of RB19 dye by the prepared NiO nanoparticles, the effect of various affecting parameters on the removal efficiency was studied and the results were presented in the following sections.

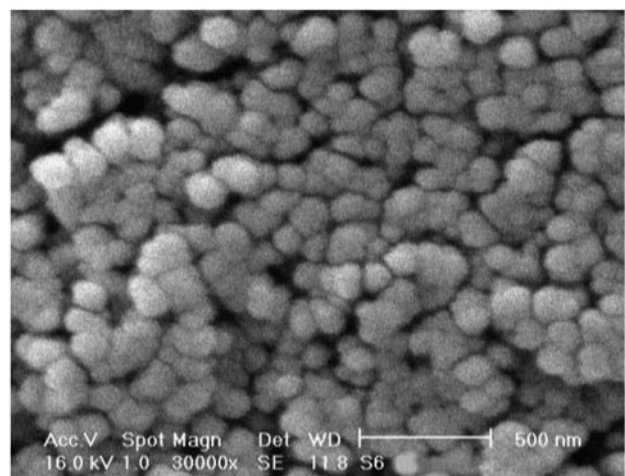


Fig. 3. The SEM image of the prepared NiO nanoparticles.

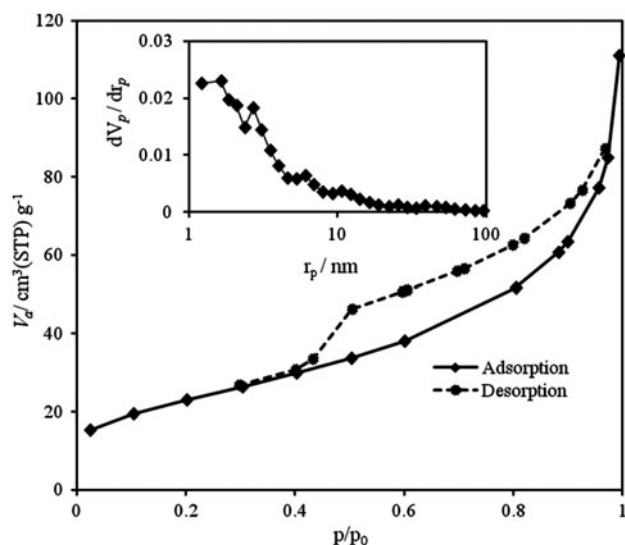


Fig. 4. N₂ adsorption/desorption isotherm curve of NiO nanoparticles and BJH pore size distribution plot (inset).

Table 2
Surface properties of NiO nanoparticles

Properties	Values
BET surface area	81.59 m ² g ⁻¹
Total pore volume, V _p	0.16 cm ³ g ⁻¹
Average pore diameter	8.07 nm
BJH average pore diameter, r _p	1.64 nm

3.2.1. Effect of initial pH of solution

To investigate the effect of initial pH on the RB19 adsorption onto NiO, 0.10 g portions of NiO nanoparticles were treated separately with 50 mL of RB19 solutions of different concentrations (75, 150, and 300 mg L⁻¹) at various pHs ranging from 3 to 12 for 60 min, while the other conditions were kept constant. As shown in Fig. 5, the removal efficiency of RB19 is almost constant over the entire range of the experimental pHs and the same trend is seen for the dye solutions with different concentrations, indicating the solution pH has no significant influence on the dye adsorption. Adsorption behavior of RB19 onto NiO nanoparticles may be related to the presence of hydroxyl groups on the surface of metal oxides (such NiO) and the degree of their protonation/deprotonation. As it is known [39], the pH of zero point charge (pH_{ZPC}) of NiO particles is around 10.3, and hence the predominant charge on the NiO surfaces is positive at pHs < pH_{ZPC}. Therefore, at pH < 10.3, the adsorption of RB19 (an ionic dye) on the NiO surface is mainly due to ionic electrostatic attractions between the

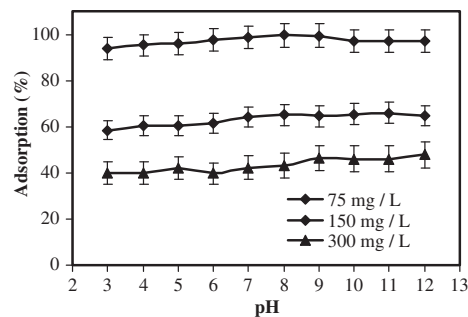


Fig. 5. Effect of pH on the removal efficiency of RB19 by NiO nanoparticles at different initial dye concentrations (adsorbent dosage = 0.10 g; contact time = 60 min).

negative sulfonyl (–SO₃) groups of RB19 molecules (Table 1) and the positively charged sites of the NiO surface. On the other hand, the efficient adsorption of RB19 onto NiO nanoparticles at pH > pH_{ZPC} suggests that in addition to ionic electrostatic attractions, other adsorption mechanisms such as hydrogen bonding may be involved. The hydrogen bonding can be due to the interactions of O atoms (–sulfonic and –ketonic groups) and N–amino groups of the RB19 molecule with –OH groups on the surface of the NiO nanoparticles. Since the solution pH had negligible effect on the RB19 adsorption, the next experiments were performed at natural pH of the RB19 solution (without pH adjustment), i.e. 6.5.

3.2.2. Effect of contact time

The effect of contact time on the removal of RB19 dye was studied by mixing 0.10 g of NiO nanoparticles with 50 mL of RB19 solution (75 mg L⁻¹) at different solution pHs and the mixture was stirred for different periods (5–120 min) of contact time. As shown in Fig. 6, the rate of adsorption is initially fast and about 80% of RB19 dye is removed within the first 5 min of contact time. Obviously, the maximum adsorption is attained after 60 min of exposure time and further increase in the contact time has no significant effect on the removal efficiency. Hence, a contact time of 60 min seems to be sufficient to achieve the equilibrium for the removal of RB19. It should be noted that the equilibrium time for the adsorption of RB19 onto NiO adsorbent is extremely shorter than the reported values for many other adsorbents [18,40,41]. The time required to achieve adsorption equilibrium is an important factor to design an adsorption system from the practical point of view, because the shorter time amounts to lower operation cost, and thus it is extensively feasible.

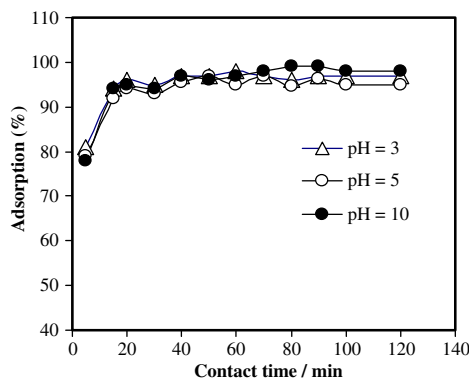


Fig. 6. Effect of contact time on the removal efficiency of RB19 by NiO nanoparticles at different pHs (adsorbent dosage = 0.10 g; initial dye concentration = 75 mg L⁻¹).

3.2.3. Effect of adsorbent dosage

The influence of adsorbent dosage on the removal of RB19 dye was studied by treating different dosages of adsorbent (0.01–0.2 g) with 50 mL of RB19 (75 mg L⁻¹) solutions for 15 min. As it is obvious (Fig. 7), the removal percentage of dye increases with the increase in the adsorbent mass and reaches the maximum value with 0.11 g of the adsorbent. No significant change is observed with further increase in the adsorbent dosages. Thus, 0.11 g of adsorbent is selected as optimum dosage. The increase in the percentage of dye removal with adsorbent mass can be attributed to the increase in the adsorbent surface area, augmenting the number of adsorption sites available for adsorption.

3.2.4. Effect of initial dye concentration

The effect of initial dye concentration on the removal efficiency of RB19 by NiO nanoparticles is shown in Fig. 8. It is evident that the adsorption

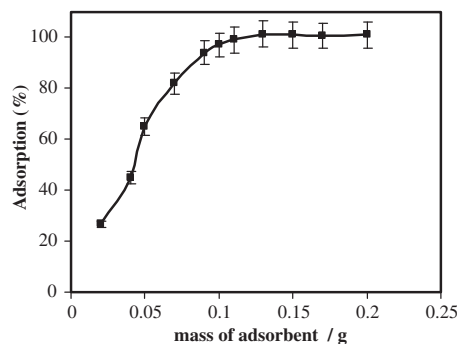


Fig. 7. Effect of adsorbent dosage on the removal of RB19 by NiO nanoparticles (initial dye concentration = 75 mg L⁻¹; contact time = 15 min).

percentage was decreased with the increase in the concentration of RB19. This is due to the fact that for a fixed adsorbent dosage, the total available adsorption sites are limited. Hence, at lower concentrations, the number of dye molecules which are available in the solution is less as compared to the available sites on the adsorbent and at higher concentrations, the available sites for adsorption become fewer. Therefore, the percentage removal of the dye is decreased when its concentration increases.

3.3. Statistical evaluation of the kinetic and isotherm parameters

The kinetic and equilibrium models were fitted using the nonlinear fitting facilities of the software Microcal Origin 7.0. In addition, the models were evaluated by an error function (F_{error}) which measures the differences in the amount of dye uptake by the adsorbent predicted by the model and the actual q measured experimentally. The F_{error} is expressed as [42]:

$$F_{\text{error}} = \sqrt{\sum \left(\frac{(q_{i,\text{cal}} - q_{i,\text{exp}})}{q_{i,\text{exp}}} \right)^2 \frac{1}{p-1}} \quad (3)$$

where $q_{i,\text{cal}}$ is the value of q predicted by the fitted model, $q_{i,\text{exp}}$ is the value of q measured experimentally, and p is the number of experiments performed.

3.4. Adsorption kinetics

To investigate the mechanism of adsorption process, the data obtained from adsorption kinetic experiments were analyzed using pseudo-first-order (Lagergren model) and pseudo-second-order kinetic models [43,44], which are expressed as follows:

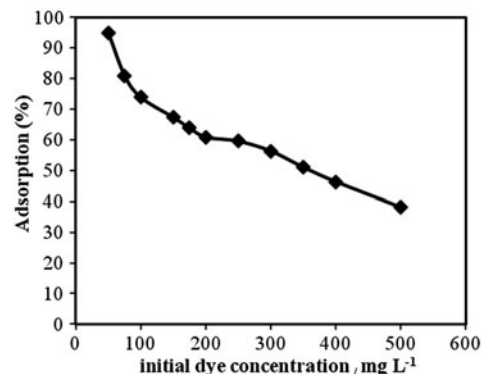


Fig. 8. Effect of initial concentration of RB19 on its removal by NiO nanoparticles (adsorbent dosage = 0.11 g; contact time = 15 min).

$$q_t = q_e[1 - \exp(-k_1 t)] \quad (4)$$

$$q_t = \frac{(k_2 \cdot q_e^2 \cdot t)}{(1 + q_e \cdot k_2 \cdot t)} \quad (5)$$

where k_1 (min^{-1}) is the pseudo-first-order rate constant and k_2 ($\text{g mg}^{-1} \text{min}^{-1}$) is the pseudo-second-order rate constant, q_e and q_t (mg g^{-1}) are the amounts of dye adsorbed at equilibrium and at any time t (min), respectively.

As shown in Fig. 9, the experimental data well fit to the pseudo-second-order rate, however, the pseudo-first-order fitted model does not produce reasonable results. Accordingly, the kinetic parameters of the pseudo-second-order fitted model are calculated and listed in Table 3. The low error function (F_{error}) value and also the high R^2 value of the pseudo second-order model suggest it as a proper kinetic model. It should be noted that only the analysis of R^2 value for the establishment of a given model is not enough, because the error function (F_{error}) evaluates the differences associated with each individual point fitted by the model, in relation to each measured experimental point. On the other hand, the R^2 value measures the differences associated with each individual point in relation to the average fitted curve [42,45]. Moreover, a good agreement between the model fit ($q_{e,\text{cal}}$) and experimentally observed equilibrium adsorption capacity ($q_{e,\text{exp}}$) values of the pseudo-second-order model demonstrates that the adsorption of RB19 onto the NiO nanoparticles can be described using the pseudo-second-order rate. These results indicate that the adsorption mechanism depends on the adsorbent and adsorbate, and rate-limiting step may be chemisorption. Similar kinetic model has also been reported for adsorption of RB19 onto other adsorbents [18,23,46].

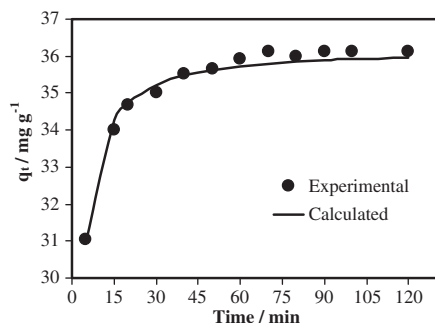


Fig. 9. Pseudo-second-order kinetic model of RB19 adsorption onto NiO nanoparticles.

3.5. Adsorption isotherms

The adsorption isotherm is an important parameter to describe the interaction of adsorbate with adsorbent and is very important for the design of an adsorption system. The equilibrium adsorption data of RB19 onto NiO nanoparticles were analyzed using the non-linear forms of Langmuir [47], Freundlich [48], and Langmuir–Freundlich (Sips) isotherms [49]. The Langmuir model assumes monolayer adsorption on a uniform surface with a finite number of adsorption sites, while the Freundlich isotherm is applicable to both monolayer (chemisorption) and multilayer adsorption (physisorption) and is based on non-ideal sorption on the heterogeneous surface. The Sips model is a combination of the Langmuir and Freundlich models. At low concentrations of the adsorbate, this model approaches the Freundlich model, which can describe the heterogeneous systems, and at high concentrations of adsorbate, it provides monolayer adsorption capacity that is the characteristic of Langmuir isotherm. The Langmuir (Eq. (6)), Freundlich (Eq. (7)), and Sips (Eq. (8)) isotherms are expressed as:

$$q_e = \frac{q_m \cdot k_L \cdot C_e}{1 + k_L C_e} \quad (6)$$

$$q_e = K_F C_e^{1/n} \quad (7)$$

$$q_e = \frac{K_s q_m C_e^{1/n}}{1 + K_s C_e^{1/n}} \quad (8)$$

where q_m is the monolayer adsorption capacity (mg g^{-1}), K_L is the Langmuir adsorption constant related to the affinity of binding sites (L mg^{-1}) of adsorbent toward the adsorbate. K_F ($\text{mg g}^{-1} (\text{L mg}^{-1})^{1/n}$) and n (dimensionless) are the Freundlich adsorption constants which refer to adsorption capacity and adsorption intensity, respectively. K_s (L mg^{-1}) is the Sips constant related to energy and affinity of adsorption.

The adsorption parameters determined by non-linear regression are listed in Table 4. Also, as an example, the fitted plots of adsorption isotherm at 25°C are shown in Fig. 10. As it can be seen from this figure, the best agreement between the experimental and model data is obtained by the Sips model. Based on the R^2 and F_{error} values listed in Table 4, the Sips isotherm with the lowest F_{error} and the high R^2 values is the best model to describe the adsorption of RB19 onto NiO nanoparticles.

As a comparison, the commercial NiO was also evaluated for RB19 adsorption under the same

Table 3

Pseudo-second-order kinetic parameters of RB19 adsorption onto NiO nanoparticles at 25°C

$q_{e,exp}$	$k_2/g\ mg^{-1}\ min^{-1}$	$q_{e,cal}\ mg\ g^{-1}$	F_{error}	R^2
36.12 ± 0.72	0.02346 ± 0.00123	42.57 ± 0.26	6.000×10^{-3}	0.9857

conditions as those of NiO nanoparticles. Adsorption experiments were performed using dye solutions with initial concentration in the range of 50–500 mg L⁻¹. The adsorption capacity of the commercial NiO was estimated to be 38.62 mg g⁻¹, which is much lower than that of the NiO nanoparticles (98.83 mg g⁻¹). The higher adsorption capacity of the prepared nano-sized NiO can be attributed to its higher surface area and lower particle size. Moreover, a comparative evaluation of the adsorbent capacity of NiO nanoparticles with various types of adsorbents for the adsorption of RB19 is given in Table 5. The monolayer adsorption capacity (q_m) of NiO nanoparticles for RB19 is relatively high compared with some adsorbents [40,41,46,50,51]. It should be noted that, although the adsorption capacity of NiO nanoparticles is lower than that of some other adsorbents [18,52,53], the adsorption capacity in our work is achieved at easy conditions such as room temperature, short contact time, and without any pH adjustment. For example, the adsorbents in reference 18 or 40 need a contact time of 4 and 5 h, respectively. Likewise, most of the adsorbents require a strongly acidic solution which could

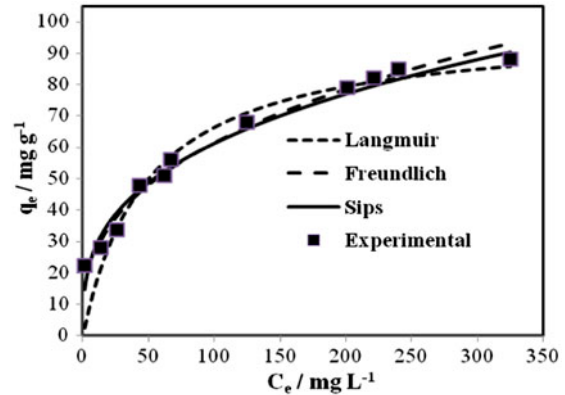


Fig. 10. Isotherm models of RB19 adsorption onto NiO nanoparticles at 25°C. (NiO dosage = 0.11 g; contact time = 60 min; initial dye concentration = 75 mg L⁻¹).

make the removal process difficult [52,53]. It should be highlighted that the adsorbent used in this study can be prepared by low-cost materials and simple procedure which is very valuable from the economical

Table 4

Isotherm parameters of RB19 onto NiO nanoparticles at different temperatures

Model	Temperature		
	25°C	35°C	45°C
<i>Langmuir</i>			
q_m (mg g ⁻¹)	98.83 ± 5.30	105.53 ± 5.48	116.50 ± 5.89
K_L (L mg ⁻¹)	0.021 ± 0.005	0.095 ± 0.008	0.230 ± 0.009
R^2	0.9797	0.9787	0.9551
F_{error}	0.2924	0.2122	0.3529
<i>Freundlich</i>			
K_F (mg/g (L/mg) ^{1/n})	13.26 ± 1.58	19.11 ± 1.04	29.18 ± 1.87
n	3.00 ± 0.21	2.99 ± 0.13	3.09 ± 0.14
R^2	0.9702	0.9672	0.9535
F_{error}	0.1327	0.1589	0.2871
<i>Sips</i>			
K_{LF} (L mg ⁻¹)	0.1097 ± 0.0130	0.1410 ± 0.0291	0.2601 ± 0.0253
q_m (mg g ⁻¹)	119.96 ± 2.05	124.02 ± 2.25	129.95 ± 2.73
n	2.99 ± 0.20	3.01 ± 0.22	2.98 ± 0.25
R^2	0.9988	0.9976	0.9989
F_{error}	0.0534	0.1145	0.1309

and practical points of view. As a result, the prepared NiO nanoparticles can be employed as alternative adsorbents for the removal of RB19 and may be considered efficient and cost-effective adsorbents in water treatment.

3.6. Effect of temperature

The effect of temperature on the adsorption of RB19 onto NiO nanoparticles was investigated by treating 0.11 g sorbent with 50 mL of dye solution (75 mg L^{-1}) at 25, 35, and 45°C under optimum conditions. The results revealed that the adsorption capacity increased with the increase in temperature, indicating that the adsorption process was endothermic in nature (Table 4). The thermodynamic parameters (ΔG° , ΔH° , ΔS°) of the adsorption process were calculated by using the following equations [55]:

$$\Delta G^\circ = -RT \ln K \quad (9)$$

$$\Delta G^\circ = \Delta H^\circ - T\Delta S^\circ \quad (10)$$

$$\ln K = -\frac{\Delta H^\circ}{RT} + \frac{\Delta S^\circ}{R} \quad (11)$$

where T is the absolute temperature (K), R is the universal gas constant ($8.314 \text{ J mol}^{-1} \text{ K}^{-1}$), K (L mol^{-1}) is the equilibrium adsorption constant of the isotherm fits [56]. The change in Gibbs's free energy change (ΔG°) was calculated using $\ln K$ values for different

temperatures (Eq. (9)). The enthalpy change (ΔH°) and entropy change (ΔS°) of adsorption were estimated from the slope and intercept of the linear plot of $\ln K$ vs. $1/T$ (Eq. (11)), respectively. The thermodynamic parameters of adsorption process are summarized in Table 6.

The positive value of adsorption enthalpy (ΔH°) indicates that the adsorption is an endothermic process. The positive value of the ΔS° demonstrate the spontaneous nature of adsorption. The positive ΔS° value indicates the increased degree of freedom of the system, suggesting randomness at the solid/liquid interface during the adsorption of RB19 onto NiO adsorbent. The positive adsorption entropy may be interrelated to the extent of dehydration of the dye molecules. During the dye adsorption onto the adsorbent, the number of water molecules surrounding the dye molecules decrease, releasing the water molecules in solution which can increase their degree of freedom. Negative values of ΔG° indicate that the adsorption of RB19 by NiO nanoparticles is a spontaneous and favorable process for all studied temperatures (Table 6).

3.7. Desorption and reuse studies

Desorption experiments were carried out to test the reusability of the adsorbent in industrial applications. The desorption experiments were performed using different desorbing solutions including sodium hydroxide, (0.1 mol L^{-1}), methanol, ethanol, and pure

Table 5
Comparison of the monolayer adsorption capacities of RB19 onto NiO nanoparticles with other adsorbents

Adsorbent	Conditions			$^a q_m$ (mg g^{-1})	Refs.
	pH	Temperature	Time		
^b CC/OPA	6	30°C	4 h	416.7	[18]
MgO nanoparticles	8	25°C	5 min	166.6	[23]
Wheat bran	1.0	20°C	300 min	97.1	[40]
Biomass rhizopus	2	Room temp.	20 h	90.0	[41]
^c MMMCNTs	d	25°C	45 min	88.80	[46]
Wood waste	1.7	–	30 min	4.75	[50]
Fungal biomass	2	30°C	60 min	80.9	[51]
Modified bentonite	1.5	20°C	60 min	124.82	[52]
Modified bentonite	1.5	20°C	–	207	[53]
Polyethyleneimine	–	20°C	–	121	[54]
Commercial NiO	d	25°C	60 min	38.62	This work
NiO nanoparticles	d	25°C	60 min	98.83	This work

^aSorption capacity.

^bCross-linked chitosan/oil palm ash composite.

^cMagnetite-modified multi-wall carbon nanotubes (MMMCNTs).

^dMagnetite-modified multi-wall carbon nanotubes (MMMCNTs).

Table 6

Thermodynamic parameters of RB19 adsorption onto NiO nanoparticles

ΔS° (J mol ⁻¹ K ⁻¹)	ΔH° (kJ mol ⁻¹)	ΔG° (kJ mol ⁻¹)		
		Temperature (K)		
		298	308	318
205.61 ± 0.04	33.84 ± 0.01	-27.59 ± 0.29	-29.16 ± 0.53	-31.73 ± 0.25

methanol-sodium hydroxide (0.1 mol L⁻¹) mixed solution (1:1). For this purpose, 10 mL of the each eluent was added to 0.1 g of the dye loaded adsorbent in a beaker and the mixture was shaken for 15 min. After filtration, the dye concentration in the desorbed solution was measured spectrophotometrically and the percentage of dye desorbed from the adsorbent was determined. From the result, the desorption efficiency was found to be 45, 72, 81, and 92% using ethanol, methanol, methanol/sodium hydroxide mixture, and sodium hydroxide, respectively. Thus, sodium hydroxide was used as proper eluent for the desorption process. After elution of the adsorbed dyes, the adsorbent was washed with deionized water and dried at 60°C overnight and reused for the dye removal. The results showed that the removal efficiency varied from 92 to 81% during the 3 cycles of adsorption/desorption experiments, which indicated that the present NiO nanoparticles could be reusable adsorbent.

4. Conclusion

NiO nanoparticles with an average size of 20 nm were studied as adsorbents for the removal of RB19 from aqueous solutions. The adsorption kinetics followed the pseudo-second-order rate and the adsorption isotherms could be described by the Sips model. The adsorption process was endothermic in nature with an enthalpy change of 33.84 kJ mol⁻¹ and entropy change of 205.61 J mol⁻¹ K⁻¹ at 298–318 K, respectively. The Gibb's free energy value increased from -27.59 to -31.73 kJ mol⁻¹ when the temperature increased from 298–318 K. The prepared NiO nanoparticles exhibited efficient adsorptive properties such as high adsorption capacity, short contact time, and independency of the solution pH for adsorption of RB19. The present NiO nanoparticles were also found to be more efficient than commercial NiO for the removal of RB19. In addition to the simple and cost-effective method for preparation of the present NiO adsorbent, its excellent adsorption properties suggested NiO nanopowder as a promising adsorbent for the removal of RB19 from wastewater.

Acknowledgment

The authors gratefully acknowledge the financial and technical support provided by the Payame Noor University.

References

- [1] H. Zollinger, *Color Chemistry Synthesis, Properties and Applications of Organic Dyes and Pigments*, VCH Publications, Weinheim, Allemagne, 1991.
- [2] Z. Eren, F.N. Acar, Adsorption of Reactive Black 5 from an aqueous solution: Equilibrium and kinetic studies, *Desalination* 194 (2006) 1–10.
- [3] S. Karcher, A. Kornmüller, M. Jekel, Anion exchange resins for removal of reactive dyes from textile wastewaters, *Water Res.* 36 (2002) 4717–4724.
- [4] D.J. Joo, W.S. Shin, J.H. Choi, S.J. Choi, M.C. Kim, M.H. Han, T.W. Ha, Y.H. Kim, Decolorization of reactive dyes using inorganic coagulants and synthetic polymer, *Dyes Pigm.* 73 (2007) 59–64.
- [5] V. Golob, A. Vinder, M. Simonic, Efficiency of the coagulation/flocculation method for the treatment of dyebath effluents, *Dyes Pigm.* 67 (2005) 93–97.
- [6] M. Koch, A. Yediler, D. Lienert, G. Insel, A. Kettrup, Ozonation of hydrolyzed azo dye reactive yellow 84 (CI), *Chemosphere* 46 (2002) 109–113.
- [7] S. Tuğç, T. Gürkan, O. Duman, On-line spectrophotometric method for the determination of optimum operation parameters on the decolorization of acid red 66 and direct blue 71 from aqueous solution by fenton process, *Chem. Eng. J.* 181–182 (2012) 431–442.
- [8] S. Tuğç, O. Duman, T. Gürkan, Monitoring the decolorization of acid orange 8 and acid red 44 from aqueous solution using Fenton's reagents by on-line spectrophotometric method: Effect of operation parameters and kinetic study, *Ind. Eng. Chem. Res.* 52 (2013) 1414–1425.
- [9] Z. Eren, Degradation of an azo dye with homogeneous and heterogeneous catalysts by sonophotolysis, *Clean —Soil Air Water* 40 (2012) 1284–1289.
- [10] G. Muthuraman, M.M. Ibrahim, Removal of anionic dye from aqueous solution using a cationic carrier, *Int. J. Ind. Chem.* 4 (2013) 15–21.
- [11] M. Belhachemi, F. Addoun, Adsorption of congo red onto activated carbons having different surface properties: Studies of kinetics and adsorption equilibrium, *Desalin. Water Treat.* 37 (2012) 122–129.
- [12] E. Ayranci, O. Duman, In-Situ UV-visible spectroscopic study on the adsorption of some dyes onto

- activated carbon cloth, Sep. Sci. Technol. 44 (2009) 3735–3752.
- [13] S. Selvakumar, R. Manivasagan, K. Chinnappan, Biodegradation and decolorization of textile dye wastewater using *Ganoderma lucidum*, Biotech 3 (2013) 71–79.
- [14] C. Lizama, J. Freer, J. Baeza, H.D. Mansilla, Optimized photodegradation of Reactive Blue 19 on TiO₂ and ZnO suspensions, Catal. Today 76 (2002) 235–246.
- [15] L.H. Ai, Y. Zhou, J. Jiang, Removal of methylene blue from aqueous solution by montmorillonite/CoFe₂O₄ composite with magnetic separation performance, Desalination 266 (2011) 72–77.
- [16] M. Turabik, B. Gozmen, Removal of basic textile dyes in single and multi-dye solutions by adsorption: Statistical optimization and equilibrium isotherm studies, Clean—Soil Air Water 41 (2013) 1080–1092.
- [17] S.B. Wang, H.T. Li, L.Y. Xu, Application of zeolite MCM-22 for basic dye removal from wastewater, J. Colloid Interface Sci. 295 (2006) 71–78.
- [18] M. Hasan, A.L. Ahmad, B.H. Hameed, Adsorption of reactive dye onto cross-linked chitosan/oil palm ash composite beads, Chem. Eng. J. 136 (2008) 164–172.
- [19] S. Karaca, A. Gürses, M. Açıkyıldız and M. Ejder (Korucu), Adsorption of cationic dye from aqueous solutions by activated carbon, Microporous Mesoporous Mater. 115 (2008) 376–382.
- [20] V.C. Srivastava, I.D. Mall, I.M. Mishra, Adsorption thermodynamics and isosteric heat of adsorption of toxic metal ions onto bagasse fly ash (BFA) and rice husk ash (RHA), Chem. Eng. J. 132 (2007) 267–278.
- [21] C.C. Chen, H.J. Fan, J.L. Jan, Degradation pathways and efficiencies of acid blue 1 by photocatalytic reaction with ZnO nanopowder, J. Phys. Chem. C 112 (2008) 11962–11972.
- [22] T. Poursaberi, M. Hassanisadi, Magnetic removal of reactive black 5 from wastewater using ionic liquid grafted-magnetic nanoparticles, Clean—Soil Air Water 41 (2013) 1208–1215.
- [23] G. Moussavi, M. Mahmoudi, Removal of azo and anthraquinone reactive dyes from industrial wastewaters using MgO nanoparticles, J. Hazard. Mater. 168 (2009) 806–812.
- [24] J. Hu, Z. Song, L. Chen, H. Yang, J. Li, R. Richards, Adsorption properties of MgO(111) nanoparticles for the dye pollutants from wastewater, J. Chem. Eng. Data 55 (2010) 3742–3748.
- [25] S. Qu, F. Huang, S. Yu, G. Chen, J. Kong, Magnetic removal of dyes from aqueous solution using multi-walled carbon nanotubes filled with Fe₂O₃ particles, J. Hazard. Mater. 160 (2008) 643–647.
- [26] W. Konicki, I. Pelech, E. Mijowska, I. Jasińska, Adsorption kinetics of acid dye acid Red 88 onto magnetic multi-walled carbon nanotubes-Fe₃C nanocomposite, Clean—Soil Air Water 42 (2014) 284–294.
- [27] K. Hayat, M.A. Gondal, M.M. Khaled, S. Ahmed, Effect of operational key parameters on photocatalytic degradation of phenol using nano nickel oxide synthesized by sol-gel method, J. Mol. Catal. A: Chem. 336 (2011) 64–71.
- [28] X.F. Song, L. Gao, Facile route to nanoporous NiO structures from the alpha-Ni(OH)₂/EG Precursor and application in water treatment, J. Am. Ceram. Soc. 91 (2008) 4105–4108.
- [29] A-F Comanescu, M. Mihaly, A. Meghea, Photocatalytic degradation of organic pollutants using NiO based materials, U.P.B. Sci. Bull. B, 74 (2012) 49–60.
- [30] B. Cheng, Y. Le, W. Cai, J. Yu, Synthesis of hierarchical Ni(OH)₂ and NiO nanosheets and their adsorption kinetics and isotherms to Congo red in water, J. Hazard. Mater. 185 (2011) 889–897.
- [31] Z. Song, L. Chen, J. Hu, R. Richards, NiO(111) nanosheets as efficient and recyclable adsorbents for dye pollutant removal from wastewater, Nanotechnology 20 (2009) 275707.
- [32] T. Zhu, J.S. Chen, X. Wen (David) Lou, (David) Lou, Highly efficient removal of organic dyes from waste water using hierarchical NiO spheres with high surface area, J. Phys. Chem. C 116 (2012) 6873–6878.
- [33] P.P. Zhang, X.M. Ma, Y.M. Guo, Q.Q. Cheng, L. Yang, Size-controlled synthesis of hierarchical NiO hollow microspheres and the adsorption for Congo red in water, Chem. Eng. J. 189–190 (2012) 188–195.
- [34] L. Ai, Y. Zeng, Hierarchical porous NiO architectures as highly recyclable adsorbents for effective removal of organic dye from aqueous solution, Chem. Eng. J. 215–216 (2013) 269–278.
- [35] M. Siddique, R. Farooq, A. Shaheen, Removal of reactive blue 19 from wastewaters by physicochemical and biological processes—A Review, J. Chem. Soc. Pak. 33 (2011) 284.
- [36] Z. Monsef Khoshhesab, M. Sarfaraz, Preparation and characterization of NiO nanoparticles by chemical precipitation method, Synth. React. Inorg. Met.-Org. Nano-Met. Chem. 40 (2010) 700–703.
- [37] B.D. Cullity, Elements of X-Ray diffraction, third ed., Addison-Wesley, Reading, MA, 1967.
- [38] J. Li, D.H.L. Ng, P. Song, C. Kong, Y. Song, Synthesis of SnO₂-activated carbon fiber hybrid catalyst for the removal of methyl violet from water, Mater. Sci. Eng. B 194 (2015) 1–8.
- [39] X.F. Song, L. Gao, Facile synthesis and hierarchical assembly of hollow nickel oxide architectures bearing enhanced photocatalytic properties, J. Phys. Chem. C 112 (2008) 15299–15305.
- [40] F. Çiçek, D. Özer, A. Özer, A. Özer, Low cost removal of reactive dyes using wheat bran, J. Hazard. Mater. 146 (2007) 408–416.
- [41] T. O'Mahony, E. Guibal and J.M. Tobin, Reactive dye biosorption by *Rhizopus arrhizus* biomass, Enzyme Microb. Technol. 31 (2002) 456–463.
- [42] B. Royer, N.F. Cardoso, E.C. Lima, T.R. Macedo, C. Airoidi, Sodic and acidic crystalline lamellar magadite adsorbents for the removal of methylene blue from aqueous solutions: Kinetic and equilibrium studies, Sep. Sci. Technol. 45 (2010) 129–141.
- [43] S. Lagergren, About the theory of so-called adsorption of soluble substances, K. Sven. Vetén, Hand 24 (1898) 1–39.
- [44] Y.S. Ho, G. McKay, Pseudo-second order model for sorption processes, Process Biochem. 34 (1999) 451–465.
- [45] M.I. El-Khaiary, G.F. Malash, Common data analysis errors in batch adsorption studies, Hydrometallurgy 105 (2011) 314–320.
- [46] T. Madrakian, A. Afkhami, N. Rezvani Jalal, M. Ahmadi, Kinetic and thermodynamic studies of the adsorption of several anionic dyes from water samples

- on magnetite-modified multi-walled carbon nanotubes, Sep. Sci. Technol. 48 (2013) 2638–2648.
- [47] I. Langmuir, The adsorption of gases on plane surfaces of glass, mica and platinum, J. Am. Chem. Soc. 40 (1918) 1361–1403.
- [48] H.M.F. Freundlich, Over the adsorption in solution, J. Phys. Chem. 57 (1906) 385–471.
- [49] R. Sips, On the structure of a catalyst surface. II, J. Chem. Phys. 18 (1950) 1024–1027.
- [50] A. Azizi, M.R. Alavi Moghaddam, M. Arami, Applications of wood waste for removal of reactive blue 19 from aqueous solutions: Optimization through response surface methodology, Environ. Eng. Manage. J. 11 (2012) 795–804.
- [51] M. Iqbal, A. Saeed, Biosorption of reactive dye by loofa sponge-immobilized fungal biomass of *Phanerochaete chrysosporium*, Process Biochem. 42 (2007) 1160–1164.
- [52] Ö. Gök, A.S. Özcan, A. Özcan, Adsorption behavior of a textile dye of Reactive Blue 19 from aqueous solutions onto modified bentonite, Appl. Surf. Sci. 256 (2010) 5439–5443.
- [53] A. Özcan, Ç. Ömeroğlu, Y. Erdoğan, A.S. Özcan, Modification of bentonite with a cationic surfactant: An adsorption study of textile dye Reactive Blue 19, J. Hazard. Mater. 140 (2007) 173–179.
- [54] M.H. Liao., W.C. Chen., W.C. Lai, Magnetic nanoparticles assisted low-molecular weight polyethyleneimine for fast and effective removal of reactive blue 19, Fresen. Environ. Bull. 15 (2006) 609.
- [55] T. Calvete, E.C. Lima, N.F. Cardoso, J.C.P. Vaghetti, S.L.P. Dias, F.A. Pavan, Application of carbon adsorbents prepared from Brazilian-pine fruit shell for the removal of reactive orange 16 from aqueous solution: Kinetic, equilibrium, and thermodynamic studies, J. Environ. Manage. 91 (2010) 1695–1706.
- [56] Y. Liu, Is the free energy change of adsorption correctly calculated? J. Chem. Eng. Data 54 (2009) 1981–1985.